CrossMark

RESEARCH PAPER

Numerical simulation of arc and droplet transfer in pulsed GMAW of mild steel in argon

M. Hertel[1] · S. Rose[1] · U. Füssel[1]

Abstract The process capability of gas metal arc welding (GMAW) processes is mainly determined by the arc properties and the material transfer. In recent years, numerical methods are being used increasingly in order to understand the complex interactions between the arc and material transfer in gas metal arc welding. In this paper, we summarize a procedure to describe the interaction between an arc and a melting and vaporizing electrode. Thereafter, the presented numerical model is used to investigate the arc properties and the metal transfer for a pulsed GMAW process of mild steel in argon. The results of the numerical simulation are compared with OES measurements as well as high-speed images at different times in the pulse cycle and show excellent agreement. The results illustrate the high influence of the changing vaporization rate on the arc attachment at the wire electrode in the high current phase. It could be shown that a substantial part of the current does not participate in the constriction of the wire electrode via the resulting lorentz force which explains the nearly spatter-free droplet detachment in pulsed GMAW processes of mild steel in argon shielding gas.

✉ M. Hertel
Martin.Hertel@tu-dresden.de

[1] Technische Universität, Dresden, Germany

1 Introduction

Gas metal arc welding (GMAW) is one of the most common welding processes used to join a wide range of metallic materials. In GMAW, an electric arc is established between a continuously fed consumable wire and the workpiece while the process is shielded by a gas. Usually, the wire has an anodic and the workpiece a cathodic polarity. Due to the heating effect of the arc, the electrodes are melted, leading to formation of droplets at the wire electrode. These droplets are detached from the wire electrode under the influence of an electromagnetic pinch force. During the heating of the wire electrode, a high amount of metal vapor is generated which is afterwards transported through the center of the arc. Due to the varying shapes of the wire electrode and the metal vaporization, there are strong interactions between the arc and the material transfer, which mainly determine the processes capabilities of GMAW. In the future, a detailed knowledge of these complex interactions is necessary to enable further process enhancements and to meet increasing requirements.

Numerous experimental and numerical studies have been carried out to understand the interactions between the arc and the vaporizing wire electrode in GMAW. Many of these investigations are summarized by Murphy [1]. Spectroscopic investigations on GMAW arcs [2–6] show that the temperature distribution differs significantly from those of TIG arcs. For arcs in pure argon, the temperature was found to have a local radial minimum on the arc axis. Siewert et al. [7] determine shapes and temperature distributions of the wire electrode and the droplets for the system argon-iron. Furthermore, the surface tension of the wire material is determined as a function of temperature by the use of the oscillating drop method [7]. The results show that the surface tension is higher than the value previously assumed in numerical models [8–16].

Springer

Nevertheless, many process determining factors such as the heat flux to the electrode surfaces or the current path and the resulting electromagnetic forces cannot be determined by experimental methods. Furthermore, a detailed process diagnostic is complicated due to the material transfer. Therefore, numerical methods are being used increasingly to improve process understanding. In earlier models of GMAW processes [8–10], the influence of metal vapor was not considered. This results in major differences between experimentally and numerically determined process variables, e.g. the temperature distribution in the arc or the wire and droplet shapes. Schnick et al. [11, 12] present a numerical investigation of a stationary GMAW arc in which they point out that the high radiative emission of iron vapor causes a minimum in the radial temperature distribution. In their treatment, Schnick et al. use an interface tracking technique with analytical defined and time-variant shapes for the electrodes. The comparison of the numerical calculated temperature profiles in the arc via optical emission spectroscopy (OES) of Zielinska [3] shows a very good agreement. Furthermore, it is pointed out that the characteristics of the arc, e.g. the current path and the attachment of the arc at the wire electrode, dramatically change with increasing vaporization rates [12]. Krivtsun et al. [13] present a complex model of the electric charge transfer in the anode region of an evaporating anode and couple it with a simplified arc model in which the changes in the electrode shapes are omitted as well [14]. In accordance to [11, 12], it becomes evident that the arc attachment at the wire electrode is essentially determined by the metal vaporization.

The most complex models of the GMAW-process [15, 16] contain a self-consistent calculation of the vaporization of the wire electrode on the basis of the local wire surface temperature and consider the influence of metal vapor on the thermophysical and radiation properties of the plasma. The change in the electrode shapes is considered as well by using an interface capturing technique based on the volume of fluid (VOF) method by Hirt and Nichols [17].

In this article, we summarize a numerical model to describe the complex interaction between a metal vapor enriched arc and a melting and vaporizing wire electrode. By the use of this model, a pulsed GMAW process of mild steel in argon shielding gas is being investigated and compared to OES measurements and high-speed images at different times in the pulse cycle.

2 Droplet transfer model

The described model focuses on the detailed description of the droplet detachment in GMAW and is based on the simulation software ANSYS CFX. In order to reduce the computational effort, we assume rotational symmetry and omit the weld seam structure. The surface of the workpiece and melt is assumed to be flat. Detached droplets can leave the computational domain

by defining suitable boundary conditions at the bottom of the computational domain. Figure 1 shows a schematic illustration of the computational domain used.

In the model, the interaction between the wire electrode and the arc is described by a multiphase formulation based on the VOF method by Hirt and Nichols [17]. The solid and molten regions of the wire are considered as incompressible liquid phase, while the shielding gas and arc plasma are considered as compressible gaseous phase. The liquid and gaseous phases are immiscible and are separated by a free surface which corresponds to the shape of the wire electrode and the droplet. The solid regions of the electrode are modeled by a high viscosity and an additional holding force to avoid unphysical flow.

The multiphase model is combined with equations of electric potential and magnetic vector potential in order to consider the electromagnetic effects inside the wire electrode and the plasma. In the gaseous phase, we consider the influence of metal vapor which is formed at the molten wire electrode and is calculated self-consistently on the basis of the Hertz–Knudsen–Langmuir equation. For each phase, a separate energy conservation equation is solved and these are coupled by a heat transfer term at the free surface. A detailed description of the equation system used can be found in [16].

In order to improve the reliability of the droplet detachment model, we include temperature-dependent thermophysical properties from [18, 19] for the metal regions. Furthermore, we consider the temperature-dependant surface tension for the system argon-iron determined by Siewert et al. [7] whose values are much higher (1.6 to 1.8 Nm) than the constant value of 1.2 Nm used in previously numerical models [8–16].

In contrast to the formulation in [16], we include an improved weighting function from Shu [20] on the basis of the level set function, see Fig. 2. Using this improved weighting function, the multiphase properties can be calculated independently of the mesh resolution. Furthermore, it is more resistant
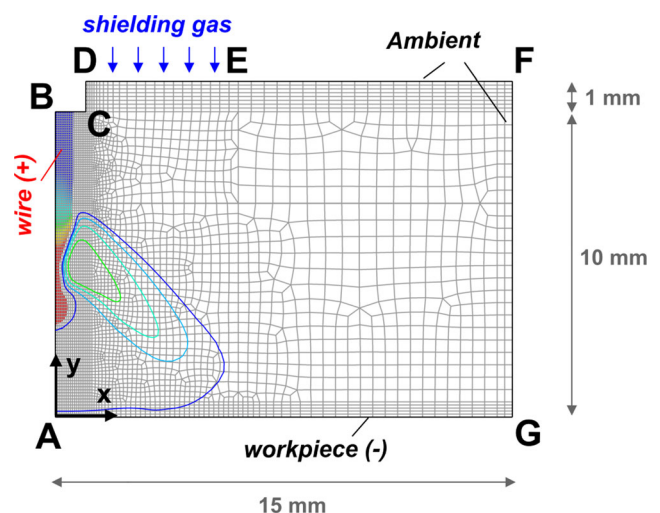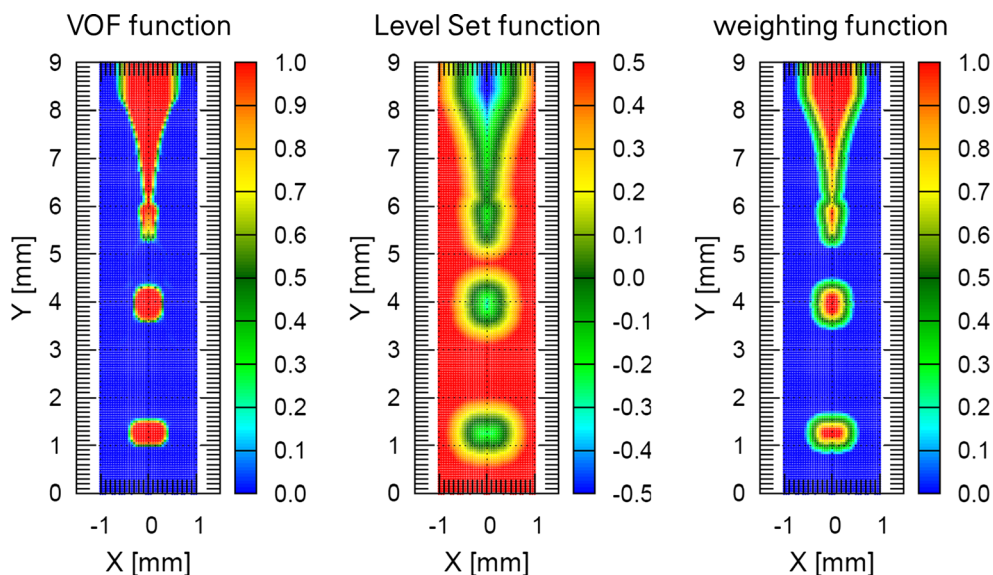

Fig. 1 Computational domain of the droplet transfer model

Fig. 2 Comparison of the regular weighting function on the basis of the VOF function (*left*) and the new weighting function (*right*) based on the level set function (*middle*)

to small calculation errors in the VOF function and therefore increases the model stability enormously.

Recently, the reliability of the droplet transfer model was improved by including a complex radiative transfer model based on the P_1 method. The band-averaged coefficients for the argon-iron plasma are taken from previous investigations [21]. By taking into account radiative transfer, the reliability of the model in the edge region of the arc could be improved significantly.

3 Calculation of a pulsed GMAW process and validation

In order to verify the calculated arc characteristics of the droplet transfer model, OES measurements on pulsed GMAW processes of Rouffet et al. [4] and Kozakov et al. [6] are used. Furthermore, the calculated electrode and droplet shapes are compared with high-speed images of Rose [22].

In the OES measurement of [4] and [6] as well as the high-speed images of [22], a pulsed GMAW process with identical parameters is used. These process parameters are shown in Table 1 and were used for the following investigations.

**Table 1** Parameter of the investigated pulsed GMAW process

Parameter	Value
Frequency | pulse time	100 Hz | 10 ms
Pulse current | ground current | mean current	420 A | 50 A | 125 A
Wire diameter	1.2 mm
Shielding gas	100 % Argon
Wire material | base material	G3Si1 | S235 JG2
Wire feeding speed | welding speed	4 m/min | 0.3 m/min
Distance contact tip—workpiece	15 mm

The current run as well as the times used for the validation with OES measurements and droplet shapes is shown in Fig. 3. In the droplet transfer model, this current profile is used as a boundary condition for the charge conservation equation at the wire inlet. To ensure that the results are not affected by the initial condition of the model, a plurality of pulse cycles was calculated to get a regular state in time. To get the results presented below, calculations of at least ten pulse cycles were required.

In Fig. 4, the calculated temperature (left side of the pictures) and iron mass fraction (right side of the pictures) distribution for different times in the pulse cycle are presented. At the beginning of the pulse cycle, the mass fraction of iron in the arc is limited to maximal 5 % and the arc attachment is concentrated at the wire tip. With increasing current, the iron vaporization at the wire tip increases while iron is transported by the flow field through the arc core. At the beginning of the high current phase (0.8 ms), the average mass fraction of iron in the arc core is about 30 %. The high radiative emission of iron leads to a minimum in the radial temperature distribution. The calculated temperatures in the arc core are between 8 000 and 10 000 K. At the edge regions of the arc, a maximum temperature of about 16 000 K is calculated.

During the high current phase (0.8 ms–1.6 ms), the evaporation rate of the wire electrode increases and thus the diameter of the substantially colder arc core is expanded. The reason for this dramatic increase of the iron vaporization is the heating of the wire surface by absorbed electrons. The heat input by absorbed electrons at the wire surface follows the instantaneous current and is in the high current phase about eight times higher than in the background current phase (1890 vs. 234 W). In addition to the constant amount of absorbed electrons in the high current phase, the resistance heating in the wire increases from about 750 W at the beginning of the high current phase up to 1300 W at the end of the high current phase. This circumstance is caused both by the onset of constriction of the wire
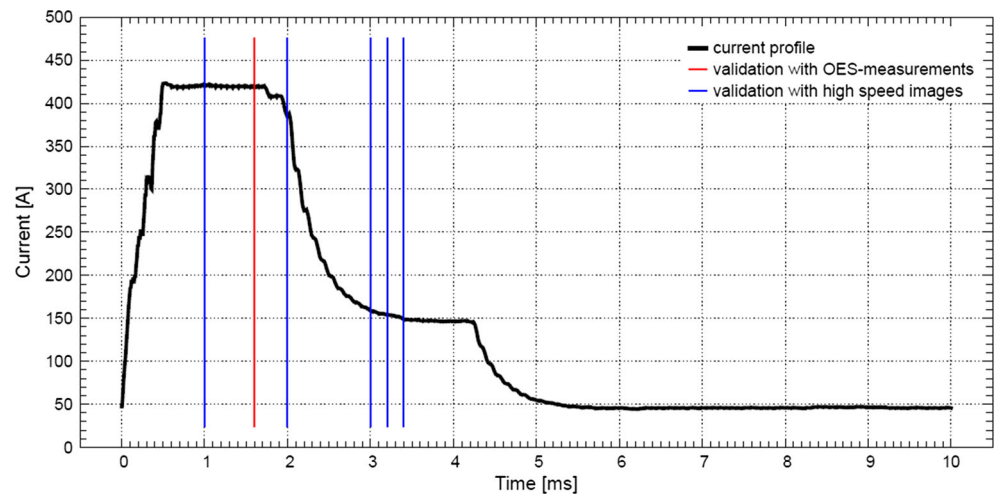
electrode and also by the decrease of the temperature-dependent electrical conductivity while heating up the wire electrode.

As a result of the increasing iron vaporization at the wire electrode, the arc attachment at the wire is shifted upwards to the contact tip. This effect could be illustrated calculating the current path in terms of a relative current by Eq. (1) [14]. By integration of the axial component of the current density j_y $(x;$ $y)$ from the axis of rotation A $(0, y)$ to the respective point of view P (x, y) within a plane in the arc at the axial position y, the current between the axis and the specific point can be

calculated. In Fig. 5, isolines of this current related to the actual current in the pulse cycle using Eq. (1) are shown.

$$I_{rel} = -\frac{2\pi \int_0^x j_y \, x \, dx}{I(t)} \qquad (1)$$

Consequently, results between the rotation axis and the green line corresponds to a current flow of 40 % of the instantaneous current. Particularly, interesting is the fact that at the time the wire constriction begins (2.4 ms), the majority of the

Fig. 4 Calculated arc temperature distribution (left) and iron mass fraction (right) for various times within the pulse cycle
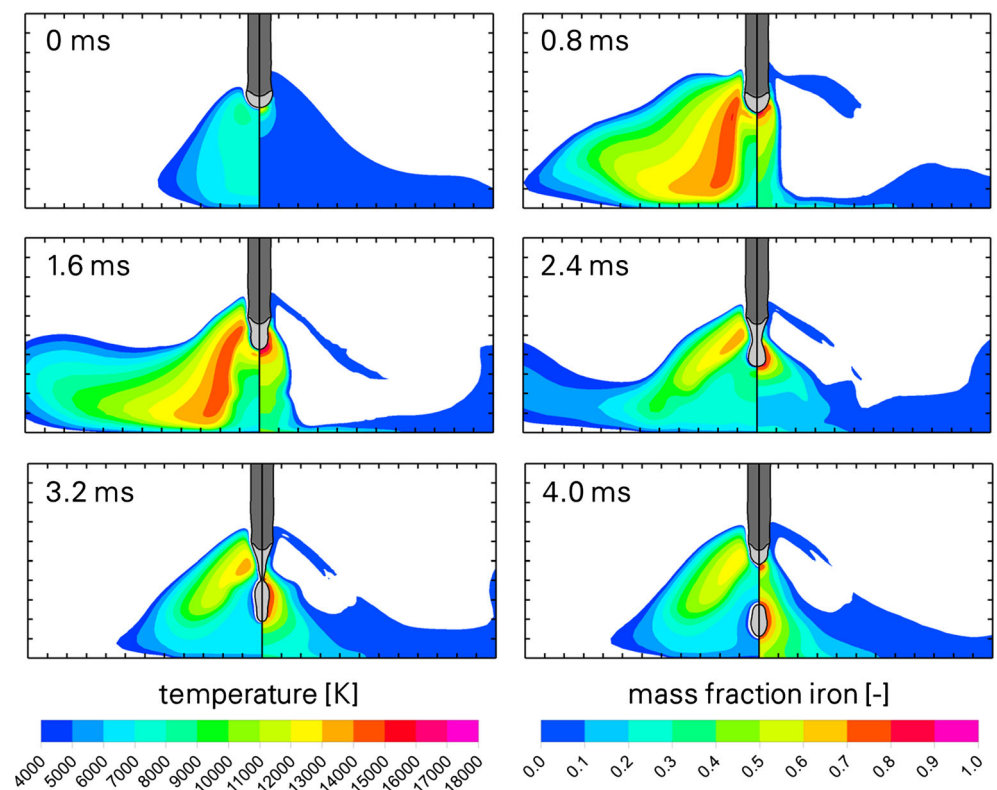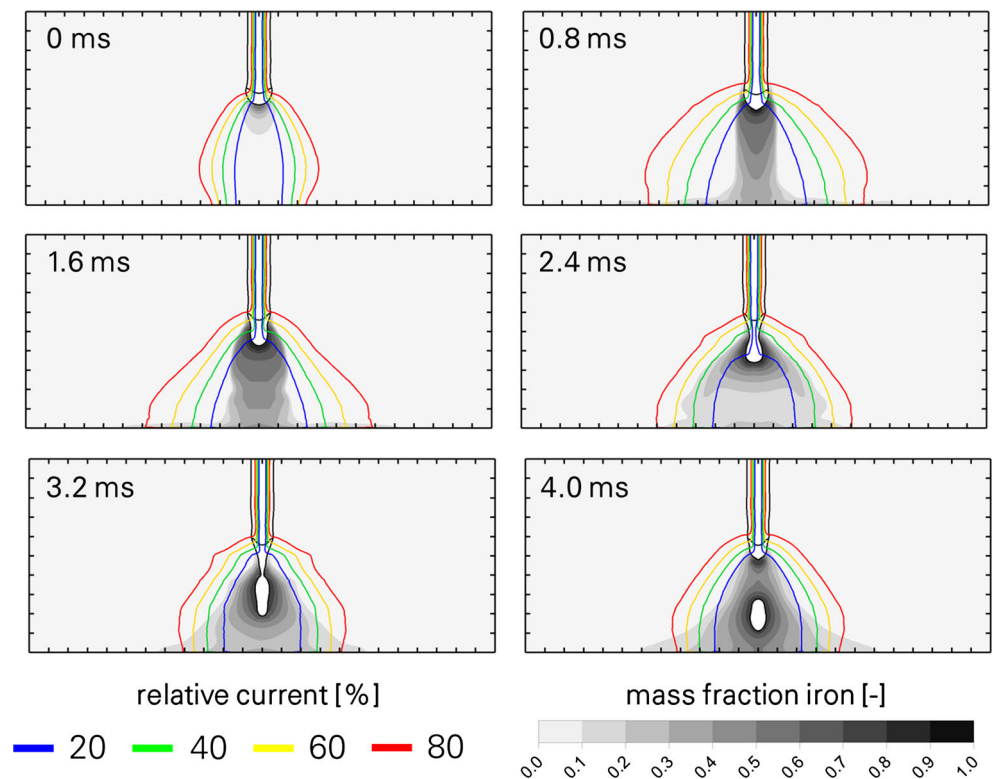
Fig. 5 Calculated current path and iron mass fraction for various times within the pulse cycle

current (about 60 %) is transported above the constriction point. Therefore, the amount of the current which is transported through the constriction area and powers the constriction of the wire electrode is substantially lower than the value of the instantaneous current. Shortly, before the droplet detachment (3.2 ms) less than 10 % of the instantaneous current is transported through the constriction area. This small current is transported through the constriction, and therefore the reduced electric pinch force in this region is the reason for the spatter-free droplet detachment in pulsed GMAW of mild steel in argon shielding gas.

After the droplet detachment, the majority of the current (over 80 %) is transported in the edge areas of the arc, where the mass fraction of iron is less than 10 %. The calculated plasma temperatures in the arc core are around 8000 K and in the edge region about 13 000 K. Around the vaporizing droplet, a layer with a high amount of iron vapor is formed, which has an iron mass fraction up to 80 %. The continuing mass flow of vaporizing iron at the droplet surface limits the heat input from the surrounding plasma. This reduction of heat input by an insulating vapor layer is called Leidenfrost effect.

In order to verify the calculated arc characteristics of the droplet transfer model, OES measurements of [4, 6] are used, see Fig. 6. The presented radial profiles of temperature and iron mass fraction were determined at the end of the high current phase approximately 2 mm above the

workpiece surface. The comparison with the numerical results shows a very good agreement for the temperature as well as the iron mass fraction, see Fig. 6 left and right. Both the temperature in the arc core as well as the approximately linear decrease in temperature with radius in the edge region can be predicted very well by the droplet transfer model. Thus, the differences in temperature are of maximal 2000 K in the edge regions of the iron core.

Regarding the iron mass fraction, it can be seen that the radius of the iron core as well as the mass fraction inside the iron core can be predicted very well and that numerical predictions lie within the experimental uncertainties.

Additionally, the calculated electrode and droplet shapes are compared with high-speed images of Rose [22] for different times in the pulse cycle, see Fig. 7. It can be seen that there is a very good agreement concerning the wire and droplet shapes. The biggest differences exist with respect to the length of the forming droplets, which tends to be too large in the calculations. This is obviously caused by an overestimation of the axial velocity in the model, forcing molten material into the droplet. This additional momentum acts against the surface tension, thus deforming the droplet. This overestimated axial velocity likely is caused by inaccuracies in the material properties used, especially the dynamic viscosity. The period of time in the pulse cycle, in which the droplet detachment takes place (period from 3.2 to 3.4 ms) can be predicted very
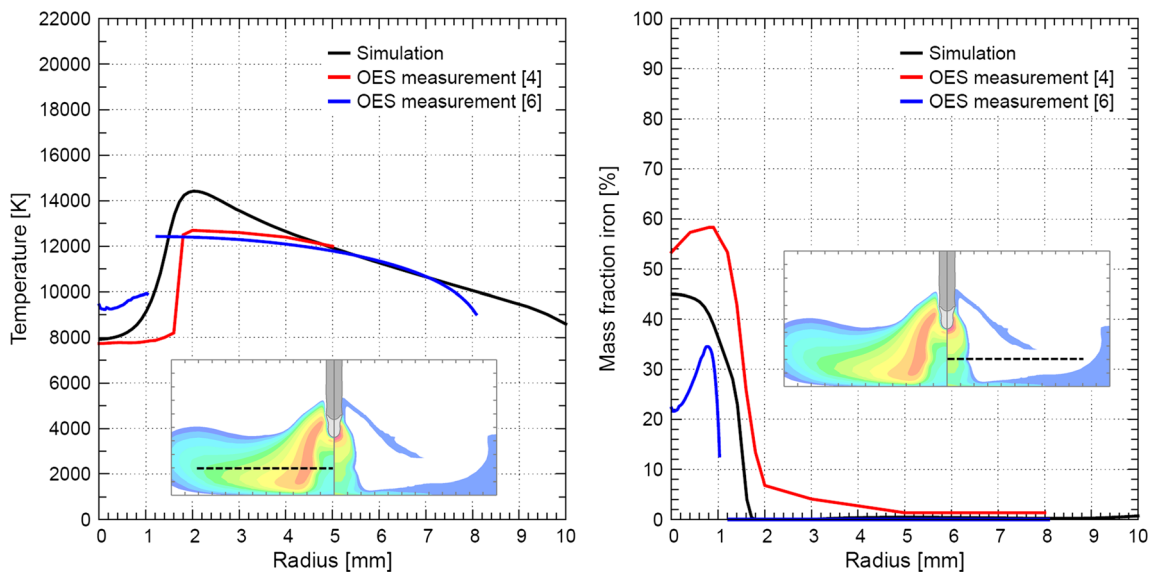
Fig. 6 Calculated radial profiles of temperature (*left*) and iron mass fraction (*right*) in comparison to OES measurements from [4] and [6]

well by the droplet transfer model. In addition, the calculated distance between the workpiece surface and the wire tip at the start of the pulse cycle and thus the energy balance in the wire electrode can be reproduced with a high accuracy.

4 Conclusions

In this article, a numerical model based on the simulation software ANSYS CFX to describe the complex interaction between a metal vapor enriched arc and a melting and
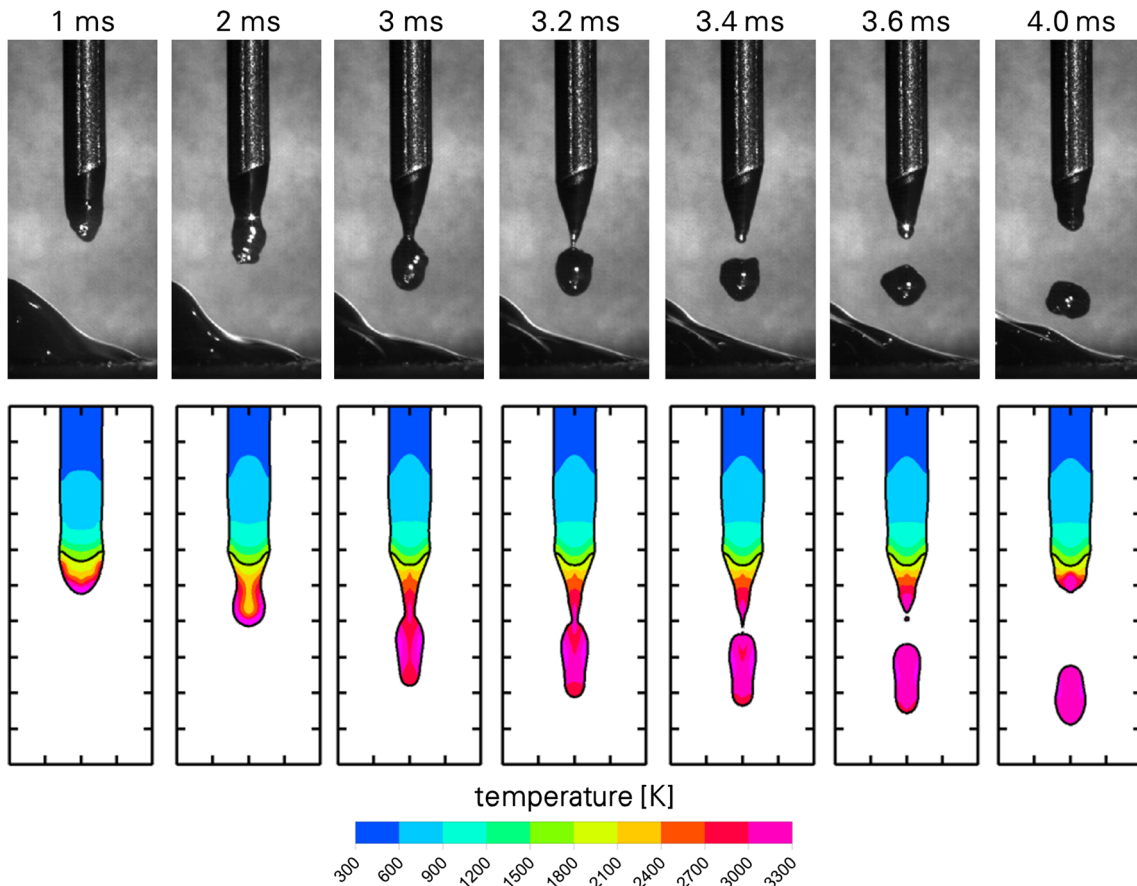

Fig. 7 Calculated shapes and temperature distributions in the metal for various times in the pulse cycle in comparison to high-speed images from Rose [22]

vaporizing wire electrode has been summarized. By the use of this model, a pulsed GMAW process of mild steel in argon shielding gas has been investigated and compared to OES measurements and high-speed images. The comparisons to these different experimental datasets show very good overall agreements.

The results illustrate that the arc attachment at the wire electrode is shifted upwards to the contact tip as a result of the increasing iron vaporization during the high current phase. The metal vaporization is mainly caused by the high heat input by absorbed electrons at the wire surface, which is nearly eight times higher in the high current phase than in the background current phase. At the time of droplet detachment, less than 10 % of the instantaneous current is transported through the constriction area. This small current flow through the constriction, and therefore the reduced electric pinch force in this region leads to the spatter-free droplet detachment in pulsed GMAW of mild steel in argon shielding gas.

The continuing mass flow of vaporizing iron from the detached droplet surface limits the heat input from the surrounding plasma, similar to the Leidenfrost effect.

References

1. Murphy AB (2010) The effects of metal vapour in arc welding. J Phys D: Appl Phys 43:434001
2. Goecke SF (2004) Auswirkungen von Aktivgaszumischungen im vpm-Bereich zu Argon auf das MIG-Impulsschweissen von Aluminium. Dissertation TU Berlin
3. Zielinska S, Musiol K, Dzierzega K, Pellerin S, Valensi F, de Izarra C, Briand F (2007) Investigations of GMAW plasma by optical emission spectroscopy. Plasma Sources Sci Technol 16:832
4. Rouffet ME, Wendt M, Goett G, Kozakov R, Schöpp H, Weltmann KD, Uhrlandt D (2010) Spectroscopic investigation of the high-current phase of a pulsed GMAW process. J Phys D: Appl Phys 43:434003
5. Tsujimura Y and Tanaka M (2013) Plasma diagnostics in gas–metal arcs during welding. IIW Conference Denver 2012, SG 212-meeting, IIW Doc. 212-1237-12
6. Kozakov R, Gött G, Schöpp H, Uhrlandt D, Schnick M, Hässler M, Füssel U, Rose S (2013) Spatial structure of the arc in the pulsed GMAW process. J Phys D: Appl Phys 46:224001
7. Siewert E, Schein J, Forster G (2013) Determination of enthalpy, temperature, surface tension and geometry of the material transfer in PGMAW for the system argon–iron. J Phys D: Appl Phys 46: 224008
8. Haidar J, Lowke JJ (1996) Predictions of metal droplet formation in arc welding. J Phys D: Appl Phys 29(12):2951
9. Fan HG, Kovacevic R (2004) A unified model of transport phenomena in gas–metal arc welding including electrode, arc plasma and molten pool J. Phys D: Appl Phys 37:2531
10. Xu G, Hu J, Tsai HL (2009) Three-dimensional modeling of arc plasma and metal transfer in gas metal arc welding. Int. J. Heat Mass Transfer 52:1709–1724
11. Schnick M, Füssel U, Hertel M, Spille-Kohoff A, Murphy AB (2010) Metal vapour causes a central minimum in arc temperature in gas–metal arc welding through increased radiative emission. J Phys D: Appl Phys 43:022001
12. Schnick M, Füssel U, Hertel M, Haessler M, Spille-Kohoff A, Murphy AB (2010) Modelling of gas–metal arc welding taking into account metal vapour. J Phys D: Appl Phys 43:434008
13. Krivtsun I, Demchenko V, Lesnoi A, Krikent I, Poritsky P, Mokrov O, Reisgen U, Zabirov A, Pavlyk V (2010) Modelling of electromagnetic processes in system'welding arc—evaporating anode': I. Model of anode region. Sci Technol Weld Joining 15:457–462
14. Krivtsun I, Demchenko V, Lesnoi A, Krikent I, Poritsky P, Mokrov O, Reisgen U, Zabirov A, Pavlyk V (2010) Modelling of electromagnetic processes in system 'welding arc—evaporating anode': II. Model of arc column and anode metal. Sci Technol Weld Joining 15:463–467
15. Boselli M, Colombo V, Ghedini E, Gherardi M, Sanibondi P (2012) Two-dimensional time-dependent modelling of fume formation in a pulsed gas metal arc welding process. J Phys D: Appl Phys 46: 224006
16. Hertel M, Spille-Kohoff A, Füssel U, Schnick M (2013) Numerical simulation of droplet detachment in pulsed gas–metal arc welding including the influence of metal vapour. J Phys D: Appl Phys 46: 224003
17. Hirt CW, Nichols BD (1981) Volume of fuid (vof) method for the dynamics of free boundaries. J Comput Phys 39:201–225
18. Radaj D (1999) Schweißprozesssimulation: Grundlagen und Anwendung. Verlag für Schweißen und verwandte Verfahren DVS-Verlag, Düsseldorf
19. Dilthey U, Reisgen U, Warmuth P (1999) MAGM-Hochleistungsschweißen mit Massiv- und Fülldrähten. Schweißen Schneiden Band 51:139–143
20. Shu B, Dammel F, Stephan P (2007) Implementation of the Level Set Method into Open-FOAM for Capturing the Free Interface in Incompressible Fluid Flows. OpenFOAM International Conference, Old Windsor
21. Hertel M, Spille-Kohoff A, Füssel U and Rose S (2013) Numerical simulation of radiative transfer in GMAW. IIW Conference Essen 2013, SG 212-meeting, IIW Doc. 212-1294-13
22. Rose S (2013) Einfluss des Werkstoffübergangs auf das dynamische Prozessverhalten beim Metallschutz-gasschweißen. Dissertation TU Dresden